PFC/JA-90-19

Calculated Collective Thomson Scattered Spectra from Energetic Ions in Tokamaks

D. Y. Rhee, J. S. Machuzak, P. P. Woskov, D. R. Cohn
Plasma Fusion Center, Massachusetts Institute of Technology

R. C. Myer
Applied Science and Technology, Inc.

December 31, 1990

Calculated Collective Thomson Scattered Spectra from Energetic Ions in Tokamaks *

D. Y. Rhee J. S. Machuzak P. P. Woskov
D. R. Cohn
Massachusetts Institute of Technology
Plasma Fusion Center
R. C. Myer
Applied Science and Technology, Inc.

December 31, 1990

Abstract

A new numerical code that calculates the collective Thomson scattered spectrum with a completely arbitrary distribution function was developed to model scattered spectra in ICRF heated and DT burning plasmas. Theoretical scattered spectra from energetic ions in tokamak plasmas (TFTR, JET, and Alcator C-Mod) are calculated. Calculated spectra for non-thermal minority He^3 ions in ICRF heated plasmas along with results from Maxwellian distributions are shown. Also preliminary results of calculated spectra for alpha-particles with slowing down distribution are presented.

*This work supported by DoE contract No. DEAC0278ET51013.

Contents

List of Figures

1 Introduction

A number of high power collective Thomson scattering experiments for measurements of confined energetic ions in tokamaks are in the planning or conceptual design stages which will depend heavily on theoretical calculations of the collective Thomson scattering spectral density function, $S(\mathbf{k},\omega)$. In the past, $S(\mathbf{k},\omega)$ has been calculated analytically for only a few velocity distribution functions, such as the Maxwellian. However, plasma physics theory predicts that present and future tokamak experiments may have ion distribution functions which will be highly non-Maxwellian and complex in nature because of ICRF and neutral beam heating, and the presence of alpha particles in D-T burning devices.

This paper will present a method to calculate $S(\mathbf{k},\omega)$ semi-analytically for arbitrary ion velocity distribution functions using Laguerre and Hermite orthogonal polynomials. $S(\mathrm{k},\omega)$ using the electrostatic approximation given by Sheffield is used as starting point of the derivation[2]. $S(\mathrm{k},\omega)$ will be calculated for theoretically expected ICRF heating ion velocity distribution functions in TFTR, JET and Alcator C-Mod. The results are compared with an analytic model using Maxwellian ion velocity distribution functions. Also as a benchmark test, a subtracted Maxwellian distribution function which creates an inverted velocity profile in the low velocity region, is used to calculate $S(\mathrm{k},\omega)$ and the results are compared with an existing analytic model[1]. And finally, preliminary results are presented from the study on scattering in D-T plasma by modeling the α-particle slowing down distribution.

2 $S(\mathbf{k},\omega)$ in terms of expanded f(v)

The spectral density function, $S(\mathbf{k},\omega)$, is needed in the theoretical calculation of Thomson scattered power [2]. Calculations of theoretical scattered power and signal to noise ratio is presented in another article [3]. $S(\mathbf{k},\omega)$ is defined as,

$$S(\mathbf{k},\omega) = \frac{1}{VT}\left\langle \frac{|n_e(\mathbf{k},\omega)|^2}{n_{eo}} \right\rangle = S_e + S_{i1} + S_{i2} + \ldots, \tag{1}$$

where the fluctuation wave number, $\mathbf{k}$, is,

$$\mathbf{k} = |\mathbf{k_s} - \mathbf{k_i}| \cong 2\,k_i \sin(\theta/2), \tag{2}$$

and k_i is the magnitude of the incident wave and θ is the scattering angle between $\mathbf{k_i}$ and $\mathbf{k_s}$.

For a Maxwellian velocity distribution, $S(\mathbf{k},\omega)$ is known analytically, but for more complex distributions, $S(\mathbf{k},\omega)$ is very difficult to calculate analytically. In order to treat non-Maxwellian distributions, a general form of $S(\mathbf{k},\omega)$ is derived by expanding the distribution function in terms of the Laguerre and Hermite polynomial series. Hence an arbitrary function composed of a series of Laguerre and Hermite polynomials can be used to fit a known form of a given particle distribution function by calculating the coefficients of the Laguerre and Hermite polynomial series. The initial distribution function can be in either analytic or numerical form. This fitted distribution function is then used to calculate $S(\mathbf{k},\omega)$.

An arbitrary distribution function can be expressed as a sum of Laguerre, $\mathrm{L_m}(y)$, and Hermite, $\mathrm{H_n}(x)$, polynomials,

$$f(x,y) = \sum_m \sum_n a_{mn} \mathrm{L_m}(y) \mathrm{H_n}(x) e^{-y/2} e^{-x^2/2}, \tag{3}$$

since these polynomials satisfy orthogonality conditions[4],

$$\int_0^\infty \mathrm{L_m}(y) \mathrm{L_n}(y) e^{-y} = \delta_{mn}, \tag{4}$$

and,

$$\int_{-\infty}^{\infty} \mathrm{H_m}(x) \mathrm{H_n}(x) e^{-x^2} = \sqrt{\pi} 2^m m! \delta_{mn}, \tag{5}$$

where δ_{mn} is the Kronecker delta function. Taking advantage of these orthogonality conditions, a_{mn} can be calculated,

$$a_{mn} = \int_0^\infty g_n(y) \mathrm{L_m}(y) e^{-y/2} dy, \tag{6}$$

where,

$$g_n(y) = \frac{1}{2^n n! \sqrt{\pi}} \int_{-\infty}^{\infty} f(x,y) \mathrm{H_n}(x) e^{-x^2/2} dx, \tag{7}$$

where $f(x,y)$ can be any model distribution function. Maxwellian like distribution functions typically can be accurately approximated by 10 to 20 a_{mn} coefficients. Most distribution functions modeled so far required at most a few hundred coefficients, which represents less than 100 seconds of the Cray computing time. For a Maxwellian distribution, only the a_{00} term is needed and all other higher order coefficients are zeroes.

Hence, by appropriately choosing the a_{00} term, the equations derived here become exactly the equations for the Maxwellian case.

It should be pointed out that presence of sharp cutoffs in a distribution function like that of the slowing down α-particle distribution with no energies greater than the birth energy requires many a_{mn} coefficients to model, and gives rise to the Gibbs phenomenon which causes erroneous results at the cutoff.

Using the arbitrary distribution function (Equation 3), a generalized form of the fully magnetized spectral density function is derived. A full derivation is presented in the appendix, and only the final result is presented here. Normalized variables are defined in the calculation of the $S(\mathbf{k},\omega)$ with an arbitrary distribution function are as follows,

$$t \equiv \frac{\sqrt{2}v_{\|}}{\sigma_{\|}} \quad , \quad y \equiv \frac{2v_{\perp}^2}{\sigma_{\perp}^2}$$
$$\beta_j \equiv \frac{k_{\perp}\sigma_{\perp j}}{\sqrt{2}\Omega_j} \quad , \quad \zeta_l \equiv \frac{\omega - l\Omega_j}{k_{\|}\sigma_{\|j}},$$

where $\sigma_{\|} = \sqrt{\frac{2T_{\|}}{m}}$ and $\sigma_{\perp} = \sqrt{\frac{2T_{\perp}}{m}}$. Using these normalized variables and the arbitrary form of the distribution function (Equation 3), the spectral density function is,

$$S(\mathbf{k},\omega) = \overbrace{\pi^2|1 - \frac{H_e}{\epsilon_L}|^2 \sum_l \sum_m \sum_n \sigma_{\perp e}^2 \sigma_{\|e} (a_{mn})_e \frac{\mathrm{H_n}(\sqrt{2}\zeta_l)\, e^{-\zeta_l^2}}{k_{\|}\sigma_{\|e}} \boldsymbol{\mathcal{L}}(l,m)}^{\text{electron term}}$$
$$+ \overbrace{\pi^2 Z_{eff}|\frac{H_e}{\epsilon_L}|^2 \sum_j \sum_l \sum_m \sum_n \sigma_{\perp j}^2 \sigma_{\|j} (a_{mn})_j \frac{\mathrm{H_n}(\sqrt{2}\zeta_l)\, e^{-\zeta_l^2}}{k_{\|}\sigma_{\|j}} \boldsymbol{\mathcal{L}}(l,m)}^{\text{ion term}}, \quad (8)$$

where,

$$\boldsymbol{\mathcal{L}}(l,m) \equiv \int_0^{\infty} dy\, e^{-y/2} J_l^2(\beta\sqrt{y}) \mathrm{L_m}(y) \quad (9)$$

$$\boldsymbol{\mathcal{L}}'(l,m) \equiv \int_0^{\infty} dy\, e^{-y/2} J_l^2(\beta\sqrt{y}) \mathrm{L'_m}(y) \quad (10)$$

$$\boldsymbol{\mathcal{Z}}(\zeta_l,n) \equiv \frac{1}{\sqrt{\pi}} \int_{-\infty}^{\infty} dt\, \frac{e^{-t^2} \mathrm{H_n}(\sqrt{2}t)}{(t-\zeta_l)}. \quad (11)$$

The Gaussian quadrature integration method was used to numerically calculate the above integrals (Equations 9,10,11)[5]. The integrals of Equations 9 and 10 use 300 Gauss-Laguerre quadrature points, and the integral in Equation 11 uses 80 Gauss-Hermite quadrature points. Note that for the lowest index order, Equation 9 is a

product of modified Bessel function and an exponent, Equation 10 is zero, and Equation 11 is the plasma dispersion function.

The screening function, $H_j(k,\omega)$, is calculated as,

$$\begin{aligned} H_j(\mathbf{k},\omega) &= \frac{2\pi^{3/2}\omega_{pj}^2}{k^2\sigma_\perp^2}\sum_m\sum_n \sigma_\perp^2\sigma_\parallel a_{mn} \\ &\times \sum_l\{\frac{\sigma_\perp^2}{\sigma_\parallel^2}\boldsymbol{\mathcal{L}}(l,m)[\frac{n!}{2(n/2)!}+\frac{\zeta_l}{2}\boldsymbol{\mathcal{Z}}(\zeta_l,n)-\frac{\sqrt{2}n}{2}\boldsymbol{\mathcal{Z}}(\zeta_l,n-1)] \\ &+ [(\zeta_0-\zeta_l)\boldsymbol{\mathcal{Z}}(\zeta_l,n)(\frac{1}{2}\boldsymbol{\mathcal{L}}(l,m)-\boldsymbol{\mathcal{L}}'(l,m))]\}, \end{aligned} \tag{12}$$

where J_l is the Bessel function of the first kind of order l, and ω_{pj} is the plasma frequency of jth species. Here, the jth subscript also includes the electrons. In the derivations, the screening functions for all species, including the heavy minority ions are treated as magnetized.

With enough coefficients, the fitted function should be identical to the given input function. However because of practical limitations of finite computing power, the number of coefficients are truncated at some high order. Usually the lowest order coefficient is most significant and the higher order terms become less significant. During the analysis, the coefficients were truncated when the ratio of the high order coefficient to the zeroeth coefficient is less than 10^{-4}. It would be desirable to carry out the coefficients to even higher orders, but round off errors in the integration routine become too large and limit the calculation of the the coefficients to approximately 100 terms in Laguerre space. With functions that decrease very slowly or that have sharp cutoffs, higher order terms become more significant; and the coefficients decreases very slowly. Thus modeling these types of profiles are very difficult.

Coefficients decrease much more rapidly in the Hermite space; after about 20 terms, the ratio of the last term to the first term is about 10^{-10}. Hence expansion in the Hermite space poses no numerical problems.

3 Subtracted Maxwellian Distribution

Study of scattering from the ICRF heated plasma is the main focus of this paper; however, no analytic form of $S(k,\omega)$ currently exists, and no comparison can be made

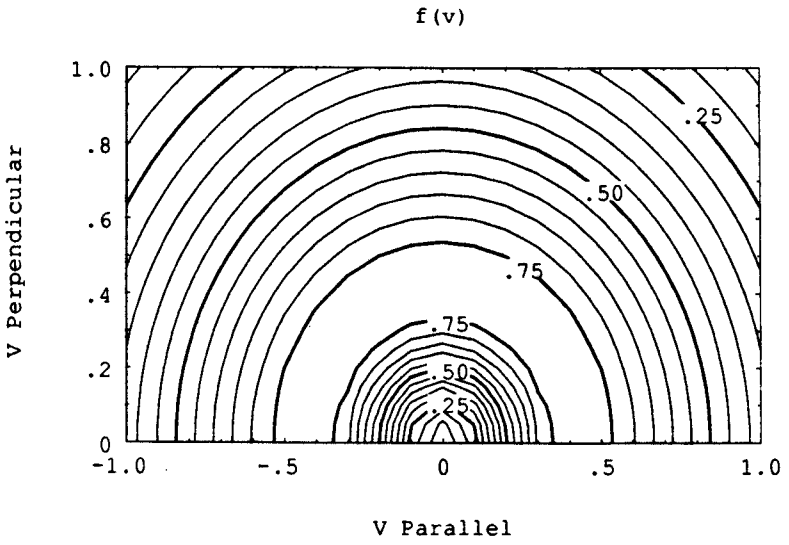

Figure 1: Contour plot of subtracted Maxwellian f(**v**) with $\gamma = 0.9, \lambda = 0.5$, and $\Gamma = 0.5$.

between the numerical model and analytic theory. Hence benchmark test of the new code using the new generalized form of $S(\mathbf{k},\omega)$ was done with an existing analytic code that uses the subtracted Maxwellian distribution. This analytic code was previously used to compare with experimental data from the Tara tandem mirror device. A detailed study of scattering in tandem mirror plasma with this model velocity profile is presented by J. Machuzak [1].

The subtracted Maxwellian distribution function used here is

$$f(v_\perp, v_\parallel) = \frac{1}{(\pi\sigma_\perp^2\sigma_\parallel)^{3/2}(1-\gamma\lambda^2\Gamma)}\left\{e^{-(v_\perp^2/\sigma_\perp^2)}e^{-(v_\parallel^2/\sigma_\parallel^2)} - \gamma e^{-(\lambda^2 v_\perp^2/\sigma_\perp^2)}e^{-(\Gamma^2 v_\parallel^2/\sigma_\parallel^2)}\right\}. \quad (13)$$

Parameters γ, λ, and Γ determine the depth and width of the hole in the low velocity region. To model a loss cone in a tandem mirror, approximate parameter values of $\gamma = .9, \lambda = .25$, and $\Gamma = 1$ should be used. However, for benchmarking purposes, $\gamma = .9, \lambda = .5$, and $\Gamma = .5$ were used to compare how effectively the fitted expansions model the given velocity distribution in both perpendicular and parallel velocity space. Ions are modeled with the subtracted Maxwellian profile, and electrons are assumed to be Maxwellian. Plasma parameters chosen model the Tara tandem mirror conditions.

Figure 1 shows the contour plot of the velocity distribution. And a plot of $S(\mathbf{k},\omega)$ spectrum is shown on Figure 2. Notice the enhanced signals in the low scattered frequency regime for the subtracted Maxwellian case in comparison to the Maxwellian case. With larger value of γ (very close to 1.) the hole in velocity space becomes deeper, and the scattered signals are even more enhanced.

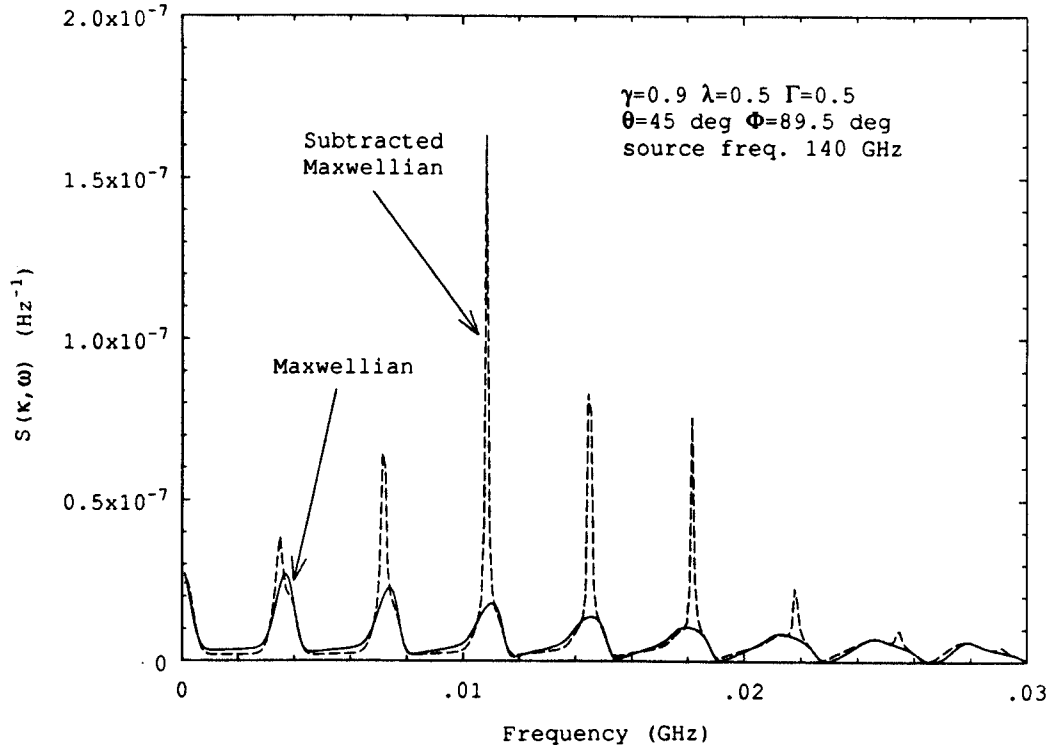

Figure 2: Comparison of $S(k,\omega)$ between Maxwellian and Subtracted Maxwellian distributions.

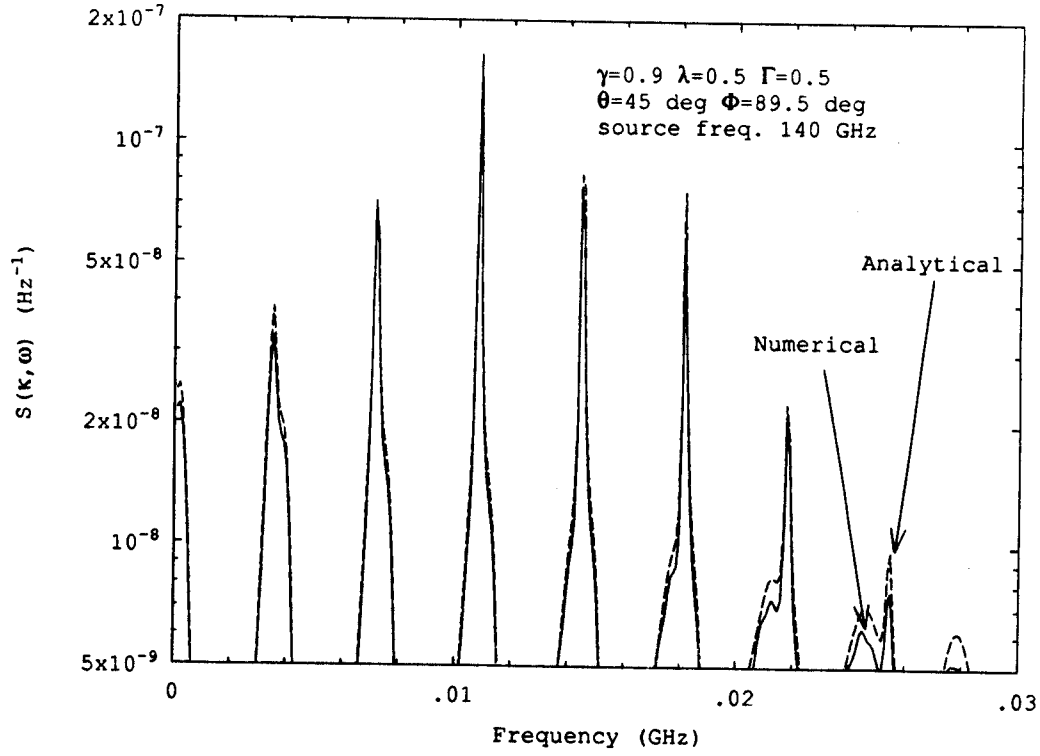

Figure 3: Comparison of $S(k,\omega)$ between Numerical and Analytical expressions of $S(k,\omega)$ for Subtracted Maxwellian distribution.

Figure 3 is a comparison of results from the subtracted Maxwellian analytic code and the numerical code using the fitted velocity profile. For this calculation, the numerical code used 60 by 10 matrix of a_{mn} coefficients. Results from the two codes match very closely, and even higher degree of accuracy can be expected if the a_{mn} coefficients were carried out to higher orders. Also, when the Maxwellian velocity distribution is modeled, the numerical results match exactly with the analytical results.

4 ICH Velocity Distribution

The new code can be used to model scattering in ICRF heated plasmas. Calculations are carried out for three experimental cases corresponding to the TFTR, JET and Alcator C-Mod tokamaks. $S(\mathbf{k},\omega)$ was calculated for 2% He^3 ICH distributions and plotted in Figures 6 through 8 along with 2% He^3 Maxwellian calculated spectra.

The bulk ions and electrons were assumed to be Maxwellian. Near the top and bottom positions of the tokamak where the tip of the He^3 particle banana orbit is in the ICRF resonance layer, the He^3 distribution is believed to be approximately anisotropic Maxwellian peaked primarily in $v_\perp$ space. Near the midplane of the tokamak, the ICH distribution is believed exhibit a 'rabbit ear' feature due to conservation of energy and angular momentum as the particles travel along the banana orbit. An approximate analytic equation, describing this 'rabbit ear' distribution at the edge and anisotropic Maxwellian distribution at the banana orbit tip, is used in the calculations [6]. This equation was used to model the 'rabbit ear' ion velocity distribution to in the calculation of $S(\mathbf{k},\omega)$. To calculate the $S(\mathbf{k},\omega)$ from a Maxwellian distribution, an analytic expression of $S(\mathbf{k},\omega)$ was used in the calculations.

The ICRF heated He^3 distribution used is,

$$f(W,\xi) = Cf_{iso}(W)[exp(\frac{-|\xi-\xi_*|}{\sigma_\xi}) + exp(\frac{-|\xi+\xi_*|}{\sigma_\xi})], \tag{14}$$

where

$$\xi = (\frac{v_\parallel}{v})_{B_{min}} = \frac{v_\parallel}{|v_\parallel|}\sqrt{1-\frac{\mu B_{min}}{W}},$$

$$\xi_* = \sqrt{1-\frac{l_q B_{min}}{\omega c m_{He^3}}},$$

$$
\begin{aligned}
\sigma_\xi &\approx \sqrt{\frac{Z_{eff}}{4A(\frac{Z_i^2}{A_i})(1+(W/W_c)^{3/2})}}, \\
\langle\frac{Z_i^2}{A_i}\rangle &= \frac{\sum_i n_i(Z_i^2/A_i)log\Lambda_i}{n_e log\Lambda_e}, \\
W &= 1/2 m_{He^3} v^2, \\
W_c &= 14.8 A T_e \langle\frac{Z_i^2}{A_i}\rangle, \\
f_{iso} &= exp(-W/T_{tail}).
\end{aligned}
$$

Here, T_{tail} is the characteristic temperature of the energetic ions as described by G. Hammett[6], B_{min} is the field strength at the location of scattering, l_q is the harmonic heating number, $\mu = 0.5 m_{He^3} v^2/B_H$, B_H is the field at the heating location, ω is the heating frequency, A is the atomic mass number, and Λ_j is the Coulomb logarithm number for the $j-j$ collision. The normalization constant, C, is determined from the following integral,

$$1 = \int_0^\infty dW \int_{-1}^{1} d\xi f(W,\xi). \tag{15}$$

For the above ICH distribution function, coefficients up to $m = 60$ and $n = 20$ indices were needed to fit to the arbitrary function (see Figure 4). The values of higher order a_{mn} coefficients decreased in magnitude very fast when compared to the a_{00} term and required only a small number of higher order coefficients.

Calculated results of scattering from the Alcator C-Mod plasma is shown on Figures 5 and 6. Results for TFTR and JET are shown on Figures 7 and 8, respectively. Figure 5 is a case with ϕ, the angle between k and B_T, very close to 90 degrees to resolve the features of electrostatic ion Bernstein waves. The bulk deuterium ion feature dominates in the low end of the spectrum. The electron feature dominates in the high frequency end, as described by the first term of the Equation 8. The lower hybrid peak is evident at the high end, which is only observable for near perpendicular scattering angles to the magnetic field, as made evident by the lack of the lower hybrid feature in Figure 6 where ϕ is 70°. At the low frequency regime of Figure 5, enhancement of the spectrum due to ion Bernstein resonances can be observed. Note that even the He^3 spectrum exhibits resonance features (< 1.5GHz), although its contribution is negligible when compared to the bulk ion and electron features. He^3 feature is dominant at the mid frequency regime between 2 to 4 GHz and is enhanced by the lower hybrid feature.

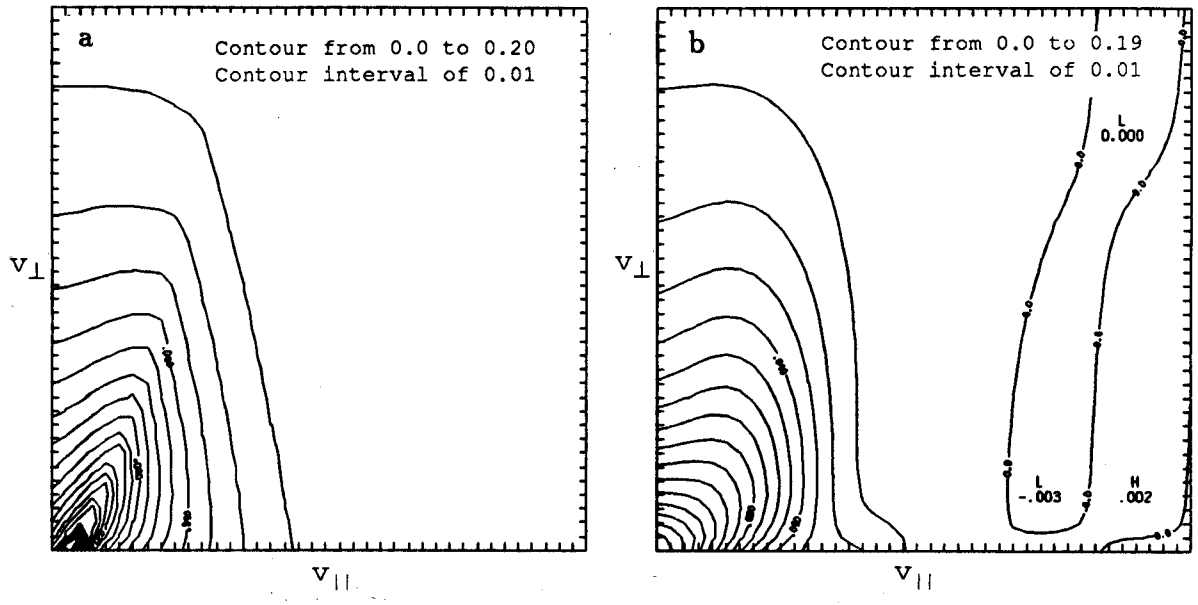

Figure 4: Contour plots of the 'rabbit ear' distribution: figure (a) is the input analytical distribution, and figure (b) is the fitted numerical distribution using $m = 60$ and $n = 20$ coefficients.

Scattering at ϕ of 70° on Alcator C-Mod, TFTR and JET are shown on Figures 6, 7 and 8, respectively. A ϕ of 70° was chosen to avoid the ion Bernstein and lower hybrid resonances and yet be still close to 90° to see the effect of the 'rabbit ear' distribution function. $S(\mathbf{k},\omega)$ curves are drawn for the cases with no He^3 present, 2% Maxwellian He^3, and 2% ICH distribution function He^3. $S(\mathbf{k},\omega)$ of ICH He^3 is about an order of magnitude less in signal strength than the case with Maxwellian He^3 for all three calculated cases. By examining the velocity space of the 'rabbit ear' ICH distribution function, this observation can be reconciled. At R_o, the major radius of the tokamak plasma center, the ICRF is tuned to match ω_{ci}, the ion cyclotron frequency, and strong perpendicular heating occurs. However, as these ions move in their banana orbits toward the outer midplane, the magnetic field is less, and $v_\perp$ decreases due to conservation of magnetic moment, and $v_{||}$ increases due to conservation of energy. Therefore, a 'rabbit ear' in velocity space occurs near the midplane of the plasma due to a depletion of high energy ions at $v_{||} \sim 0$. A high temperature Maxwellian distribution would include these ions, and consequently, the scattered power would be greater for a Maxwellian distribution function since there are more ions in the $v_{||} \sim 0$ region of velocity space compared to the ICH distribution function. If the scattering geometry were aligned to examine velocity space along the 'rabbit ear', then closer agreement with a Maxwellian distribution function is expected.

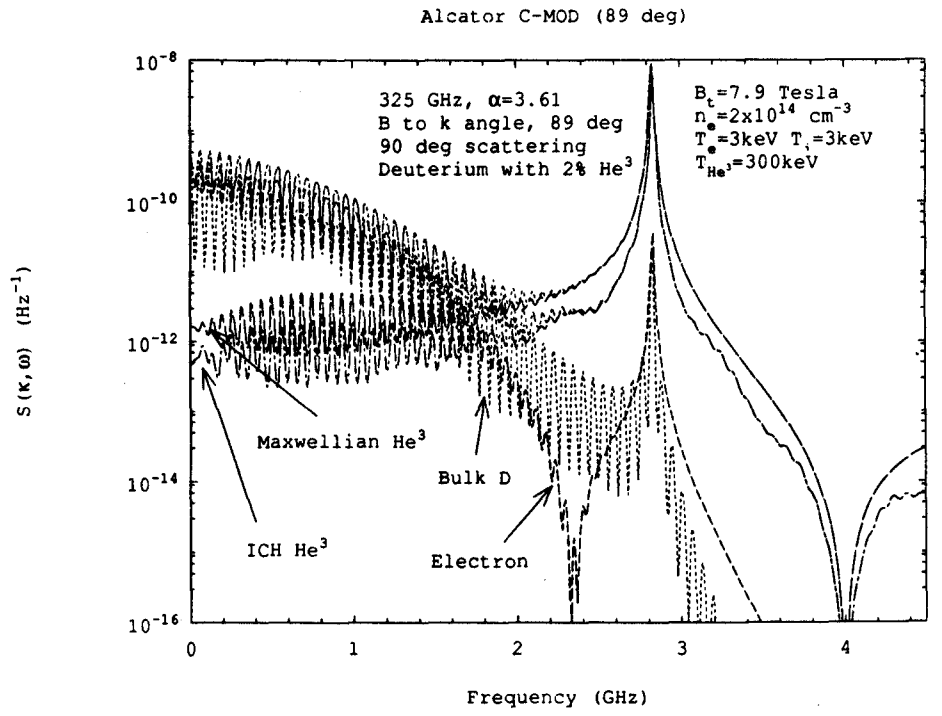

Figure 5: $S(k,\omega)$ for Alcator C-MOD: $\phi = 89.5°$

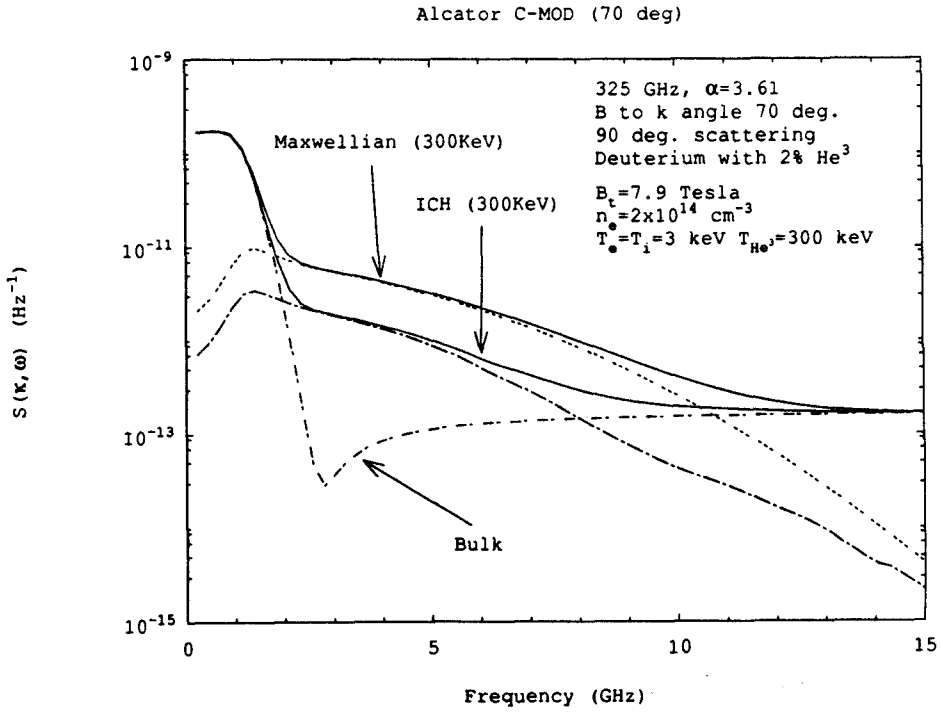

Figure 6: $S(k,\omega)$ for Alcator C-MOD: $\phi = 70.0°$

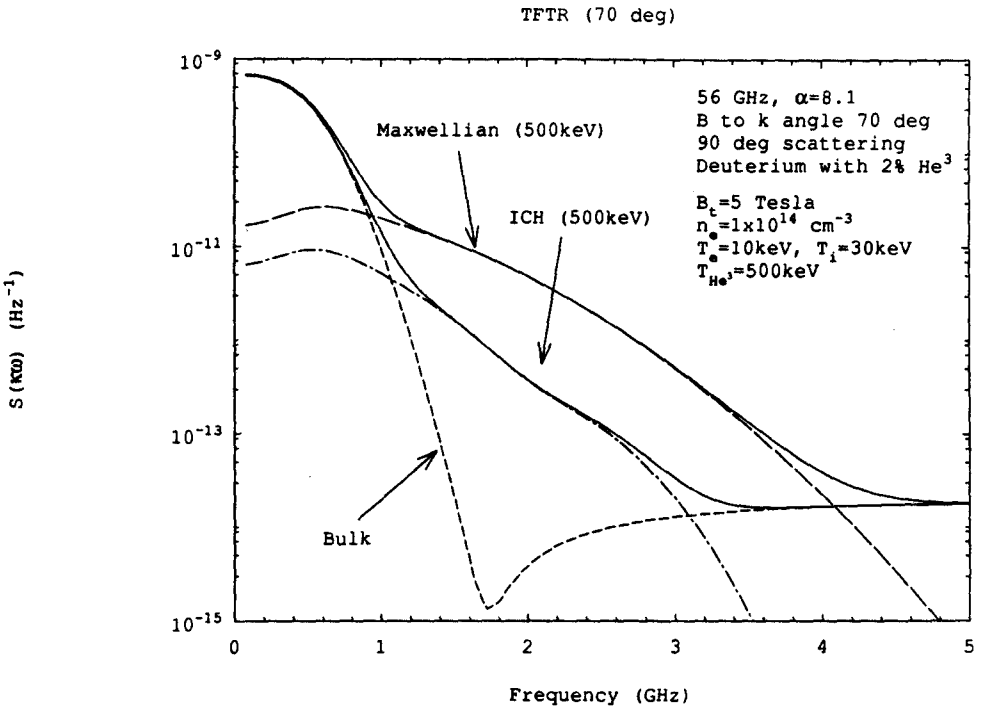

Figure 7: $S(k,\omega)$ for TFTR: $\phi = 70.0°$

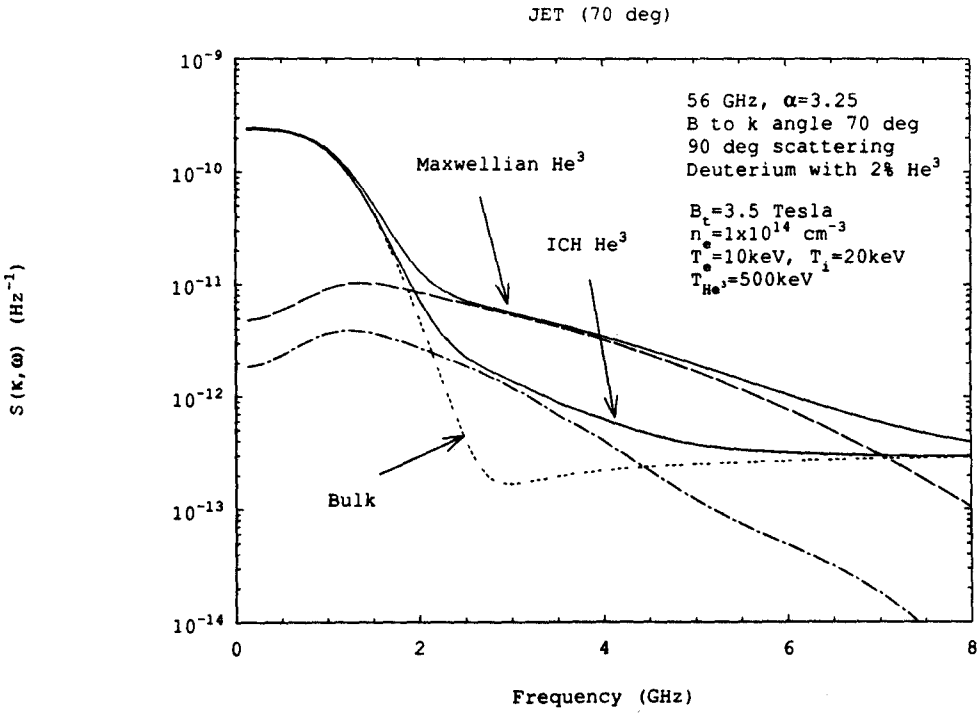

Figure 8: $S(k,\omega)$ for JET: $\phi = 70.0°$

The high frequency regime of the $S(\mathbf{k},\omega)$ is affected by the bulk electron feature, and it is sensitive to the α parameter ($\alpha \equiv 1/k\lambda_D$). This parameter is 8.11 for the present scattering calculation in TFTR and 3.25 for JET. Note that the electron feature is at least one order of magnitude greater for the JET case than for the TFTR case. Although the increase in the electron feature brings up the total $S(\mathbf{k},\omega)$, the sensitivity to the He^3 feature is decreased because the total scattered spectra is dominated by the electron feature. Hence, it is desirable to be in a regime where α is as large as possible to better resolve the He^3 feature.

5 α-particle 'Slowing Down' Distribution

A D-T burning plasma with fusion α-particles was modeled with the new code. As a benchmark, a comparison was made with an existing code that analytically models the α-particles with a slowing down distribution. Since the presence of a sharp cutoff in the distribution cannot be modeled, the slowing down distribution was modeled without the cutoff at the α birth energy. Hence the calculated scattered spectra from this model will have no roll off at the frequency corresponding to the birth energy, but the overall shape up to the cutoff should be similar to the results from the benchmark analytic model.

The slowing down velocity distribution is

$$f_\alpha(\vec{v}) = \begin{cases} 0 & ,v > v_\alpha \\ F_0/(v^3 + v_c^3) & ,v \leq v_\alpha \end{cases}$$

where $F_o = 3/[4\pi ln(1 + (v_\alpha/v_c)^3)]$, $v_c = 0.09\sigma_e$, $v_\alpha = (2E_\alpha/M_\alpha)^{1/2}$ and $E_\alpha = 3.5MeV$.

However as mentioned, the slowing down velocity distribution was modeled here without the birth energy cutoff in the numerical model. The benchmark analytical model uses the 1-dimensional form of the above slowing down distribution which takes the birth energy cutoff into account[7]. Calculated spectra for JET and TFTR cases are shown on Figures 9 and 10, respectively. The two models show reasonably good agreement, except for the absence of a roll off at 3 GHz for the numerical model. Also as a comparison, spectrum calculated by Hughes [7] is also shown on Figure 9, which closely agrees with the analytic model. Calculated results for the TFTR case is shown on Figure 10. Again, except for the absence of roll off in the numerical model, the analytical

and numerical models show reasonably good agreement. A third spectrum modeling the α-particle with a 3.5 MeV Maxwellian distribution is also shown in Figure 10.

Confined α-particles may have more flat, and possibly even inverted distributions [8]. With the numerical model, it is possible to model these distributions and calculate the scattered spectra. Again, the model may not give us a completely accurate results due to numerical limitations, but it may give us new semi-quantitative insights into scattering in a burning plasma. This analysis of scattering from confined alpha particles with distribution function other than the slowing down velocity distribution of Equation 5 will be performed in the future.

6 Conclusion

The calculation of the collective Thomson scattering spectral density function has been enhanced by the development of a theory which can accommodate arbitrary velocity distribution functions. Prior to this work, collective Thomson scattered spectra could be calculated for only a very few simple distributions which could be analytically solved, such as the Maxwellian distribution.

The ICH distribution function which models minority He^3 ions present at the midplane of tokamak plasma was used to calculate the scattered spectra. The spectral density function with this distribution indicates a decrease of an order of magnitude in scattered power from that of a simple isotropic Maxwellian distribution function of the same temperature for the orientation of the scattering wave vector to the magnetic field considered in this report. This should improve the prospects for detecting fusion alpha particles during ICH.

The analytical form derived here is adequate for the ICH distribution function, but is inadequate, at present, for the slowing down distribution function because of the sharper cut-offs in velocity space. Numerical modeling is limited by the round off errors in the calculations of high order terms. Hence input distributions with very flat slopes or sharp cut offs that require many terms in the expansions are difficult to model adequately.

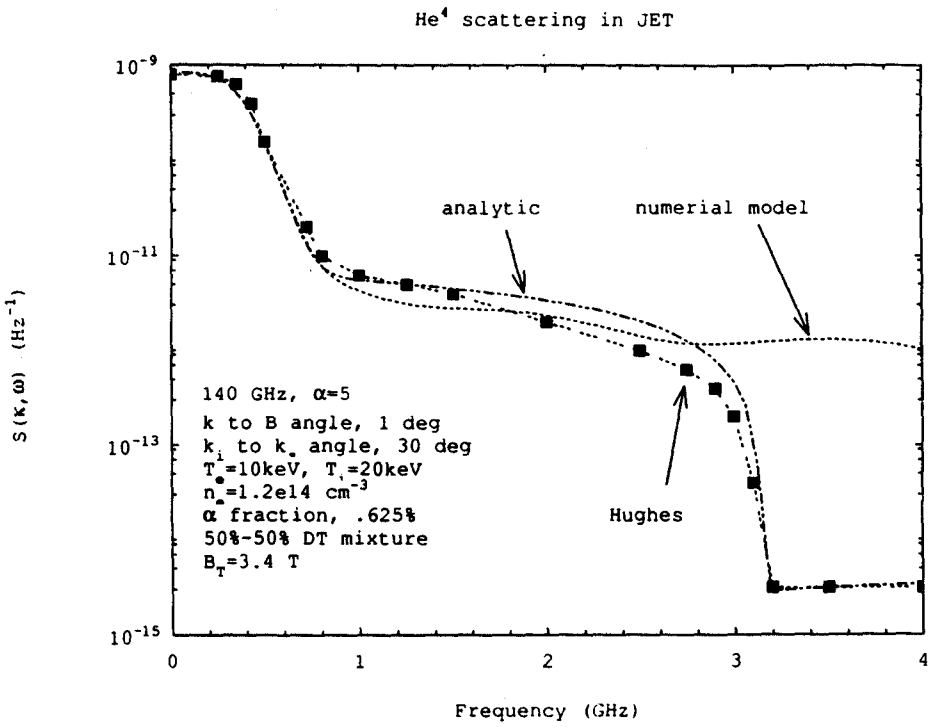

Figure 9: $S(k,\omega)$ for JET with α slowing down f(v): $\phi = 1.0°$ and $\theta = 30.0°$

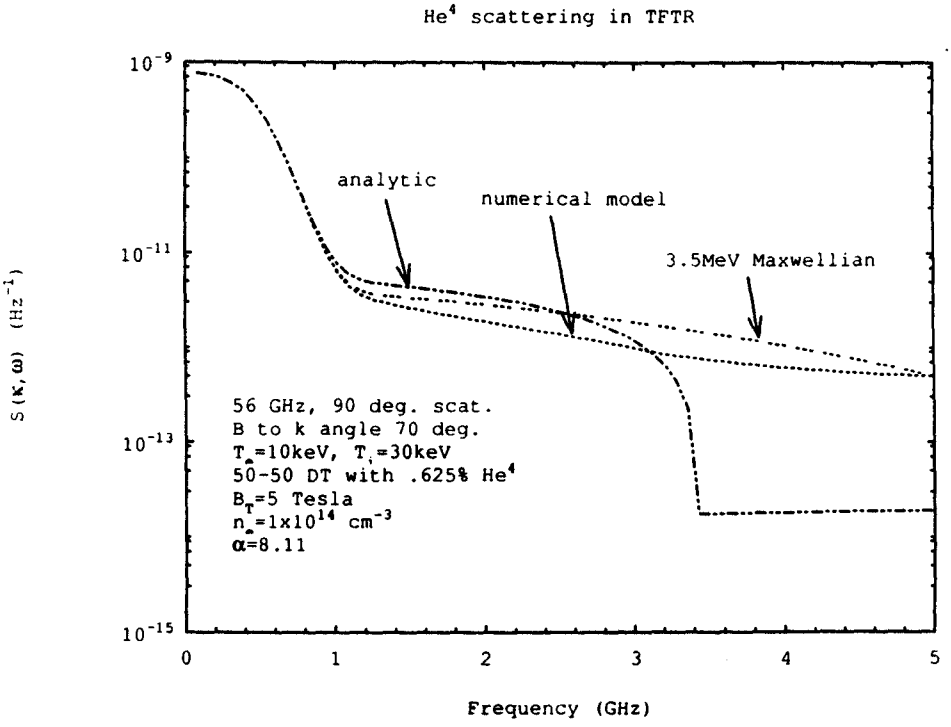

Figure 10: $S(k,\omega)$ for TFTR with α slowing down f(v): $\phi = 70.0°$ and $\theta = 90.0°$

References

[1] J.S. Machuzak Ph.D. Thesis, MIT 1990

[2] J. Sheffield, Plasma Scattering of Electromagnetic Radiation, Academic Press, New York (1975)

[3] J.S. Machuzak, D.Y. Rhee, P.P. Woskov, D.R. Cohn, R.C. Myer, Development of High Power Millimeter and Submillimeter Wavelength Collective Thomson Scattering Diagnostics for Energetic Ion Measurements in Tokamaks, Rev. Sci. Instrum. **61**, 3544 (1990)

[4] G. Arfken, Mathematical Methods for Physicists, 3rd Ed., Academic Press, Orlando, FA (1985)

[5] A.H. Stroud, D. Secrest, Gaussian Quadrature Formulas, Prentice-Hall, Englewood Cliffs, NJ (1966)

[6] G.W. Hammett, Fast Ion Studies of Ion Cyclotron Heating in the PLT Tokamak, Ph.D. Thesis, Dept. of Astrophysical Sciences, Princeton University (1986)

[7] T.P. Hughes, S.R.P. Smith, Nuclear Fusion, **28** (1988) 1451

[8] J.G. Cordey, R.J. Goldston, D.R. Mikkelsen, Nuclear Fusion, **21** (1981) 581

Appendix: Derivation of $S(k,\omega)$ with Fitted $f(\mathbf{v})$

Derivation of $S(k,\omega)$ along with H_j, following the electrostatic approximation as outlined by J. Sheffield [2], is given here. H_j, the susceptibility for jth species is given by

$$H_j(\mathbf{k},\omega) = \int_{-\infty}^{\infty} d\mathbf{v}\, \frac{4\pi e^2 n_o}{m_j k^2} \sum_l \frac{J_l^2(k_\perp \rho_j)\, \mathbf{k}\cdot \frac{\partial f_{oj}}{\partial \mathbf{v}^*}}{\omega - k_\parallel v_{\parallel j} - l\Omega_j - i\gamma} \tag{16}$$

$\mathbf{v}^*$ is Sheffield's notation in cases where f_{oj} is independent of ϕ. If the velocity is separated into $v_\perp$ and $v_\parallel$ components with respect to ϕ, then H_j can be written as

$$H_j(\mathbf{k},\omega) = \int_0^{2\pi} d\phi \int_0^{\infty} v_\perp dv_\perp \int_{-\infty}^{\infty} dv_\parallel \frac{\omega_{pj}^2}{k^2} \sum_l \frac{J_l^2(k_\perp \rho_j)\left[k_\parallel \frac{\partial f_{oj}}{\partial v_\parallel} + \frac{l\Omega_j}{v_\perp}\frac{\partial f_{oj}}{\partial v_\perp}\right]}{\omega - k_\parallel v_\parallel - l\Omega_j - i\gamma}. \tag{17}$$

Define following normalized variables and constants,

$$t \equiv \frac{2v_{\parallel j}}{\sigma_{\parallel j}} \quad , \quad y \equiv \frac{2v_{\perp j}^2}{\sigma_{\perp j}^2},$$
$$\beta_j \equiv \frac{k_\perp \sigma_{\perp j}}{\sqrt{2}\Omega_j} \quad , \quad \zeta_l \equiv \frac{\omega - l\Omega_j}{k_\parallel \sigma_{\parallel j}},$$

where,$\sigma_\perp$ and $\sigma_\parallel$ are perpendicular and parallel thermal velocities, respectively. And, defining an arbitrary distribution function in terms of Laguerre, $\mathrm{L_m}(y)$, and Hermite, $\mathrm{H_n}(t)$, polynomials,

$$f(t,y) = \sum_m \sum_n a_{mn} \mathrm{L_m}(y) \mathrm{H_n}(t) e^{-y/2} e^{-t^2/2}, \tag{18}$$

and substituting it for f_{oj} into the above equation,

$$H_j(\mathbf{k},\omega) = 2\pi \frac{\omega_{pj}^2}{k^2} \int_0^{\infty} dy \frac{\sigma_{\perp j}^2}{4} \int_{-\infty}^{\infty} dt \frac{\sigma_{\parallel j}}{\sqrt{2}} \times$$
$$\sum_l \frac{J_l^2(\beta_j\sqrt{y})}{\omega - \frac{k_\parallel \sigma_{\parallel j} t}{\sqrt{2}} - l\Omega_j} \left[\frac{\sqrt{2}k_\parallel}{\sigma_{\parallel j}} \frac{\partial}{\partial t} + l\Omega_j \frac{4}{\sigma_{\perp j}^2} \frac{\partial}{\partial y}\right] f(t,y) \tag{19}$$

$$= \frac{\pi \omega_{pj}^2}{2^{3/2} k^2} \sigma_{\parallel j} \sigma_{\perp j}^2 \int_{-\infty}^{\infty} dt \int_0^{\infty} dy \sum_m \sum_n a_{mn} \sum_l \frac{J_l^2(\beta_j\sqrt{y})}{\omega - \frac{k_\parallel \sigma_{\parallel j} t}{\sqrt{2}} - l\Omega_j} \times \tag{20}$$
$$\left\{ \frac{\sqrt{2}k_\parallel}{\sigma_{\parallel j}} \mathrm{L_m}(y) e^{-y/2} \frac{d}{dt}\left[\mathrm{H_n}(t) e^{-t^2/2}\right] + l\Omega_j \frac{4}{\sigma_{\perp j}^2} \mathrm{H_n}(t) e^{-t^2/2} \frac{d}{dy}\left[\mathrm{L_m}(y) e^{-y/2}\right] \right\}.$$

Using,

$$\frac{\partial}{\partial t}\Big[\mathrm{H_n}(t)e^{-t^2/2}\Big] = \Big[-t\mathrm{H_n}(t) + 2n\mathrm{H_{n-1}}(t)\Big]e^{-t^2/2},$$
$$\frac{\partial}{\partial y}\Big[\mathrm{L_m}(y)e^{-y/2}\Big] = \Big[-\frac{1}{2}\mathrm{L_m}(y) + \mathrm{L'_m}(y)\Big]e^{-y/2},$$

and redefining $t' \equiv t/\sqrt{2}$ and introducing ζ_l, then

$$H_j(\mathbf{k},\omega) = \frac{-\pi\omega_{pj}^2}{2k^2}\sigma_{\|j}\sigma_{\perp j}^2\sum_m\sum_n a_{mn}\int_{-\infty}^{\infty}dt'\int_0^{\infty}dy\sum_l\frac{J_l^2(\beta_j\sqrt{y})}{k_\|\sigma_{\|j}[t'-\zeta_l]}\times$$
$$\Big\{\frac{k_\|}{\sigma_{\|j}}\mathrm{L_m}(y)\Big[-2t'\mathrm{H_n}(\sqrt{2}t') + 2\sqrt{2}n\mathrm{H_{n-1}}(\sqrt{2}t')\Big] +$$
$$l\Omega_j\frac{4}{\sigma_{\perp j}^2}\mathrm{H_n}(\sqrt{2}t')\Big[-\frac{1}{2}\mathrm{L_m}(y) + \mathrm{L'_m}(y)\Big]\Big\}e^{-y/2}e^{-t'^2}. \tag{21}$$

Using the fact that $\zeta_0 - \zeta_l = \frac{l\Omega_j}{k_\|\sigma_\|}$ and defining $A_{mn} \equiv \sigma_\perp^2\sigma_\| a_{mn}$,

$$H_j(\mathbf{k},\omega) = \frac{2\pi\omega_{pj}^2}{k^2\sigma_{\perp j}^2}\sum_m\sum_n A_{mn}\int_{-\infty}^{\infty}dt'\int_0^{\infty}dy\,e^{-y/2}e^{-t'^2}\sum_l\frac{J_l^2(\beta_j\sqrt{y})}{[t'-\zeta_l]}\times$$
$$\Big\{\frac{\sigma_{\perp j}^2}{\sigma_{\|j}^2}\mathrm{L_m}(y)\Big[\frac{t'}{2}\mathrm{H_n}(\sqrt{2}t') - \frac{\sqrt{2}n}{2}\mathrm{H_{n-1}}(\sqrt{2}t')\Big] +$$
$$[\zeta_0-\zeta_l]\mathrm{H_n}(\sqrt{2}t')\Big[\frac{1}{2}\mathrm{L_m}(y) - \mathrm{L'_m}(y)\Big]\Big\}. \tag{22}$$

Rearranging the integrals in the equation,

$$H_j(\mathbf{k},\omega) = \frac{2\pi\omega_{pj}^2}{k^2\sigma_{\perp j}^2}\sum_m\sum_n A_{mn}\sum_l\Big\{\Big[\frac{\sigma_{\perp j}^2}{\sigma_{\|j}^2}\int_{-\infty}^{\infty}dt'\frac{e^{-t'^2}}{t'-\zeta_l}\times$$
$$\Big[\frac{t'}{2}\mathrm{H_n}(\sqrt{2}t') - \frac{\sqrt{2}n}{2}\mathrm{H_{n-1}}(\sqrt{2}t')\Big]\int_0^{\infty}dy e^{-y/2}J_l^2(\beta_j\sqrt{y})\mathrm{L_m}(y)\Big] +$$
$$\Big[\Big[\zeta_0-\zeta_l\Big]\int_{-\infty}^{\infty}dt'\frac{\mathrm{H_n}(\sqrt{2}t')e^{-t'^2}}{t'-\zeta_l}\times$$
$$\int_0^{\infty}dy J_l^2(\beta_j\sqrt{y})\Big[\frac{1}{2}\mathrm{L_m}(y) - \mathrm{L'_m}(y)\Big]\Big]\Big\}. \tag{23}$$

Define,

$$\boldsymbol{\mathcal{L}}(l,m) \equiv \int_0^{\infty}dy\,e^{(-y/2)}J_l^2(\beta_j\sqrt{y})L_m(y), \tag{24}$$
$$\boldsymbol{\mathcal{L}}'(l,m) \equiv \int_0^{\infty}dy\,e^{(-y/2)}J_l^2(\beta_j\sqrt{y})L'_m(y), \tag{25}$$
$$\boldsymbol{\mathcal{Z}}(\zeta_l,n) \equiv \frac{1}{\sqrt{\pi}}\int_{-\infty}^{\infty}dt\,\frac{e^{(-t'^2)}H_n(\sqrt{2}t')}{t'-\zeta_l}. \tag{26}$$

And using the relation,

$$\int_{-\infty}^{\infty} dt' \frac{t' e^{-t'^2} H_n(\sqrt{2}t')}{t' - \zeta_l} = \int_{-\infty}^{\infty} dt' e^{-t'^2} H_n(\sqrt{2}t') + \zeta_l \int_{-\infty}^{\infty} dt' \frac{e^{-t'^2} H_n(\sqrt{2}t')}{t' - \zeta_l}, \tag{27}$$

and,

$$\int_{-\infty}^{\infty} dt' e^{-t'^2} H_n(\sqrt{2}t') = \begin{cases} 0 & \text{n odd} \\ \frac{\sqrt{\pi} n!}{(\frac{n}{2})!} & \text{n even,} \end{cases} \tag{28}$$

then,

$$\begin{aligned} H_j(k,\omega) &= \frac{2\pi^{3/2}\omega_{pj}^2}{k^2\sigma_{\perp j}^2} \sum_m \sum_n A_{mn} \\ &\times \sum_l \left\{ \frac{\sigma_{\perp j}^2}{\sigma_{\| j}^2} \boldsymbol{\mathcal{L}}(l,m) \Big[\frac{n!}{2(n/2)!} + \frac{\zeta_l}{2} \boldsymbol{\mathcal{Z}}(\zeta_l, n) - \frac{\sqrt{2}n}{2} \boldsymbol{\mathcal{Z}}(\zeta_l, n-1) \Big] \right. \\ &+ \left. \Big[[\zeta_0 - \zeta_l] \boldsymbol{\mathcal{Z}}(\zeta_l, n) \Big(\frac{1}{2} \boldsymbol{\mathcal{L}}(l,m) - \boldsymbol{\mathcal{L}}'(l,m) \Big) \Big] \right\}. \end{aligned} \tag{29}$$

With $\sum_l J_l^2(x) = 1$ and,

$$\int_0^{\infty} e^{-x/2} \mathrm{L_m}(x) dx = 2(-1)^m, \tag{30}$$

then

$$\begin{aligned} H_j(k,\omega) &= \frac{2\pi^{3/2}\omega_{pj}^2}{k^2\sigma_{\perp j}^2} \sum_m \sum_n A_{mn} \\ &\times \left\{ \frac{\sigma_{\perp j}^2}{\sigma_{\| j}^2} \frac{n!(-1)^m}{(n/2)!} + \sum_l \left\{ \frac{\sigma_{\perp j}^2}{\sigma_{\| j}^2} \boldsymbol{\mathcal{L}}(l,m) \Big[\frac{\zeta_l}{2} \boldsymbol{\mathcal{Z}}(\zeta_l, n) - \frac{\sqrt{2}n}{2} \boldsymbol{\mathcal{Z}}(\zeta_l, n-1) \Big] \right. \right. \\ &+ \left. \left. \Big[\big[\zeta_0 - \zeta_l\big] \boldsymbol{\mathcal{Z}}(\zeta_l, n) \big(\frac{1}{2} \boldsymbol{\mathcal{L}}(l,m) - \boldsymbol{\mathcal{L}}'(l,m) \big) \Big] \right\} \right\} \end{aligned} \tag{31}$$

Spectral density function for a two component plasma is given as:

$$\begin{aligned} S(\mathbf{k},\omega) &= 2 \lim_{\gamma \to 0} \left\{ \gamma \left| 1 - \frac{H_e}{\epsilon_L} \right|^2 \int_{-\infty}^{\infty} \frac{d\mathbf{v} \sum_l J_l^2(k_\perp \rho_e) f_{oe}(\mathbf{v})}{(\omega - k_\| v_\| - l\Omega_e)^2 + \gamma^2} \right. \\ &\left. + Z \left| \frac{H_e}{\epsilon_L} \right|^2 \int_{-\infty}^{\infty} \frac{d\mathbf{v} \sum_m J_m^2(k_\perp \rho_i) f_{oi}(\mathbf{v})}{(\omega - k_\| v_\| - m\Omega_i)^2 + \gamma^2} \right\}, \end{aligned} \tag{32}$$

where ϵ_L is the dielectric function,

$$\epsilon_L = 1 + H_e(\kappa, \omega) + H_i(\kappa, \omega). \tag{33}$$

Using the same substitutions as $\mathrm{H_n}(\mathbf{k},\omega)$, then

$$
\begin{aligned}
S(\mathbf{k},\omega) &= 2\lim_{\gamma\to 0}\left\{\gamma\left|1-\frac{H_e}{\epsilon_L}\right|^2 2\pi\int_0^\infty\frac{\sigma_{\perp e}^2}{4}dy\int_{-\infty}^\infty\frac{\sigma_{\|e}}{\sqrt{2}}dt\times\right.\\
&\quad\sum_l J_l^2(\beta_e\sqrt{y})\sum_m\sum_n(a_{mn})_e\frac{\mathrm{L_m}(y)\mathrm{H_n}(t)e^{-y/2}e^{-t^2/2}}{(\omega-k_\|v_\|-l\Omega_e)^2+\gamma^2}\\
&+ Z\left|\frac{H_e}{\epsilon_L}\right|^2 2\pi\int_0^\infty\frac{\sigma_{\perp i}^2}{4}dy\int_{-\infty}^\infty\frac{\sigma_{\|i}}{\sqrt{2}}dt\times\\
&\quad\left.\sum_l J_l^2(\beta_i\sqrt{y})\sum_m\sum_n(a_{mn})_i\frac{\mathrm{L_m}(y)\mathrm{H_n}(t)e^{-y/2}e^{-t^2/2}}{(\omega-k_\|v_\|-l\Omega_i)^2+\gamma^2}\right\}. \qquad (34)
\end{aligned}
$$

Noting that $(\omega-k_\|v_\|-l\omega_l)^2=k_\|^2\sigma_\|^2\left[\zeta_l-t'\right]^2$, then

$$
\begin{aligned}
S(\mathbf{k},\omega) &= 2\lim_{\gamma\to 0}\left\{\gamma\left|1-\frac{H_e}{\epsilon_L}\right|^2 2\pi\int_0^\infty\frac{\sigma_{\perp e}^2}{4}dy\int_{-\infty}^\infty\frac{\sigma_{\|e}}{\sqrt{2}}dt\times\right.\\
&\quad\sum_l J_l^2(\beta_e\sqrt{y})\sum_m\sum_n(a_{mn})_e\frac{\mathrm{L_m}(y)\mathrm{H_n}(t)e^{-y/2}e^{-t^2/2}}{k_\|^2\sigma_{\|e}^2\left[\zeta_l-t'\right]^2+\gamma^2}\\
&+ Z\left|\frac{H_e}{\epsilon_L}\right|^2 2\pi\int_0^\infty\frac{\sigma_{\perp i}^2}{4}dy\int_{-\infty}^\infty\frac{\sigma_{\|i}}{\sqrt{2}}dt\times\\
&\quad\left.\sum_l J_l^2(\beta_i\sqrt{y})\sum_m\sum_n(a_{mn})_i\frac{\mathrm{L_m}(y)\mathrm{H_n}(t)e^{-y/2}e^{-t^2/2}}{k_\|^2\sigma_{\|i}^2\left[\zeta_l-t'\right]^2+\gamma^2}\right\},\\
&= \lim_{\gamma\to 0}\left\{\gamma\left|1-\frac{H_e}{\epsilon_L}\right|^2\frac{\pi\sigma_{\perp i}^2}{k_\|^2\sigma_{\|e}}\sum_m\sum_n(a_{mn})_e\sum_l\times\right.\\
&\quad\int_0^\infty dy e^{-y/2}J_l^2(\beta_e\sqrt{y})\mathrm{L_m}(y)\int_{-\infty}^\infty dt'\frac{\mathrm{H_n}(\sqrt{2}t')e^{-t'^2}}{\left[\zeta_l-t'\right]^2+\frac{\gamma^2}{k_\|^2\sigma_{\|e}^2}}\\
&+ Z\left|\frac{H_e}{\epsilon_L}\right|^2\frac{\pi\sigma_{\perp e}^2}{k_\|^2\sigma_{\|i}}\sum_m\sum_n(a_{mn})_i\sum_l\times\\
&\quad\left.\int_0^\infty dy e^{-y/2}J_l^2(\beta_i\sqrt{y})\mathrm{L_m}(y)\int_{-\infty}^\infty dt'\frac{\mathrm{H_n}(\sqrt{2}t')e^{-t'^2}}{\left[\zeta_l-t'\right]^2+\frac{\gamma^2}{k_\|^2\sigma_{\|i}^2}}\right\}. \qquad (35)
\end{aligned}
$$

Using the relation,

$$
\int_{-\infty}^\infty\frac{f(v)dv}{(v-z_{Re})^2+z_{Im}^2}=\frac{\pi}{z_{Im}}f(z_{Re}), \qquad (36)
$$

the spectral density function becomes

$$S(k,\omega) = \pi^2 \left|1 - \frac{H_e}{\epsilon_L}\right|^2 \sum_m \sum_n \sum_l (A_{mn})_e \frac{H_n(\sqrt{2}\zeta_l)\, e^{-\zeta_l^2}}{k_{\|}\sigma_{\|e}} \mathcal{L}(l,m)$$
$$+ \pi^2 Z \left|\frac{H_e}{\epsilon_L}\right|^2 \sum_m \sum_n \sum_l (A_{mn})_i \frac{H_n(\sqrt{2}\zeta_l)\, e^{-\zeta_l^2}}{k_{\|}\sigma_{\|i}} \mathcal{L}(l,m). \quad (37)$$

With multi-ion species, the spectral density function is,

$$S(k,\omega) = \pi^2 \left|1 - \frac{H_e}{\epsilon_L}\right|^2 \sum_m \sum_n \sum_l (A_{mn})_e \frac{H_n(\sqrt{2}\zeta_l)\, e^{-\zeta_l^2}}{k_{\|}\sigma_{\|e}} \mathcal{L}(l,m)$$
$$+ \pi^2 Z_{eff} \left|\frac{H_e}{\epsilon_L}\right|^2 \sum_j \sum_m \sum_n \sum_l (A_{mn})_j \frac{H_n(\sqrt{2}\zeta_l)\, e^{-\zeta_l^2}}{k_{\|}\sigma_{\|j}} \mathcal{L}(l,m). \quad (38)$$